

The S-PLUS: a star/galaxy classification based on a Machine Learning approach

M. V. Costa-Duarte^{1*}, L. Sampedro¹, A. Molino¹, H. S. Xavier¹,
F. R. Herpich¹, A. L. Chies-Santos², C. E. Barbosa^{1,3}, A. Cortesi^{1,4}, W. Schoenell²,
A. Kanaan⁵, T. Ribeiro⁶, C. Mendes de Oliveira¹, S. Akras^{4,7}, A. Alvarez-Candal⁷,
C. L. Barbosa⁸, J. L. N. Castellón^{9,10}, P. Coelho¹, M. L. L. Dantas¹, R. Dupke⁷,
A. Ederoclite¹, A. Galarza⁷, T. S. Gonçalves⁴, J. A. Hernandez-Jimenez^{1,11},
Y. Jiménez-Teja⁷, A. Lopes⁷, P. A. A. Lopes⁴, R. Lopes de Oliveira^{12,7},
J. L. Melo de Azevedo¹³, L. M. Nakazono¹, H. D. Perotoni¹, C. Queiroz¹⁴, K. Saha¹⁵,
L. Sodr e Jr.¹, E. Telles⁷, R. C. Thom de Souza¹⁶

¹Instituto de Astronomia, Geof sica e Ci ncias Atmosf ricas, Universidade de S o Paulo, 05508-090, S o Paulo, Brazil

²Departamento de Astronomia, Instituto de F sica, Universidade Federal do Rio Grande do Sul, Porto Alegre, Brazil

³Steward Observatory, University of Arizona, 933 N Cherry Ave, Tucson, AZ 85719, United States

⁴Valongo Observatory, Federal University of Rio de Janeiro, Ladeira Pedro Antonio 43, Saude Rio de Janeiro, RJ, 20080-090, Brazil

⁵Departamento de F sica, Universidade Federal de Santa Catarina, Florian polis, SC, 88040-900, Brazil

⁶NOAO, P.O. Box 26732, Tucson, AZ 85726

⁷Observat rio Nacional / MCTIC, Rua General Jos  Cristino 77, Rio de Janeiro, RJ, 20921-400, Brazil

⁸Dept. of Physics, Centro Universit rio da FEI Av. Humberto de Alencar Castelo Branco, 3972. 09850-901 S o Bernardo do Campo - SP, Brazil.

⁹Instituto de Investigacion Multidisciplinario en Ciencia y Tecnolog a, Universidad de La Serena. Benavente 980, La Serena, Chile

¹⁰Departamento de F sica y Astronom a, Universidad de La Serena. Avenida Juan Cisternas 1200, La Serena, Chile.

¹¹Departamento de Ciencias F sicas, Universidad Andr s Bello, Fern ndez Concha 700, Las Condes, Santiago, Chile

¹²Departamento de F sica, Universidade Federal de Sergipe, Av. Marechal Rondon, S/N, 49000-000, S o Crist v o, SE, Brazil

¹³Instituto de Ci ncias Matem ticas e de Computa o - Universidade de S o Paulo (ICMC-USP), S o Paulo, Brazil

¹⁴Departamento de F sica Matem tica, Instituto de F sica, Universidade de S o Paulo, SP, Rua do Mat o 1371, S o Paulo, Brazil

¹⁵Inter-University Centre for Astronomy and Astrophysics, PostBag 4, Ganeskhind, Pune-411007, India

¹⁶Universidade Federal do Paran , Campus Jandaia do Sul, Rua Dr. Jos  Maximiano, 426, Jandaia do Sul-PR, 86900-000, Brazil.

Accepted . Received ; in original form

ABSTRACT

We present a star/galaxy classification for the Southern Photometric Local Universe Survey (S-PLUS), based on a Machine Learning approach: the Random Forest algorithm. We train the algorithm using the S-PLUS optical photometry up to $r=21$, matched to SDSS/DR13, and morphological parameters. The metric of importance is defined as the relative decrease of the initial accuracy when all correlations related to a certain feature is vanished. In general, the broad photometric bands presented higher importance when compared to narrow ones. The influence of the morphological parameters has been evaluated training the RF with and without the inclusion of morphological parameters, presenting accuracy values of 95.0% and 88.1%, respectively. Particularly, the morphological parameter FWHM/PSF performed the highest importance over all features to distinguish between stars and galaxies, indicating that it is crucial to classify objects into stars and galaxies. We investigate the misclassification of stars and galaxies in the broad-band colour-colour diagram ($g-r$) versus ($r-i$). The morphology can notably improve the classification of objects at regions in the diagram where the misclassification was relatively high. Consequently, it provides cleaner samples for statistical studies. The expected contamination rate of red galaxies as a function of the redshift is estimated, providing corrections for red galaxy samples. The classification of QSOs as extragalactic objects is slightly better using photometric-only case. An extragalactic point-source catalogue is provided using the classification without any morphology feature (only the SED information) with additional constraints on photometric redshifts and FWHM/PSF values.

1 INTRODUCTION

Several astronomical surveys need to face the challenge of classifying observed sources in terms of their astronomical nature, i.e., stars, galaxies, QSOs, planetary nebulae, supernovae, among others (Robertson et al. 2015, and references therein). The classification of objects in survey catalogues could speed up considerably studies in several fields, as evidenced by the widely successful Sloan Digital Sky Survey (SDSS, York et al. 2000; Abolfathi et al. 2017) and the myriad of queries and samples made out of it. Studies on classification of astronomical sources are needed to estimate, for instance, contamination rates even for surveys that are conceived to be focused on a particular object/science case. This classification becomes more crucial for photometric surveys, where the spectral information is not available to precisely classify objects.

Apart from deep pencil-like surveys which cover small areas in the sky and large extragalactic volumes, the current generation of extragalactic surveys generally covers large areas in the sky and low/intermediate redshift ranges, e.g., Javalambre Physics of the Accelerating Universe Astrophysical Survey (J-PAS, Benítez et al. 2014), Dark Energy Survey (Dark Energy Survey Collaboration 2017), Euclid (Refregier et al. 2010) and Large Synoptic Survey Telescope (LSST, Ivezić et al. 2008), S-PLUS (Mendes de Oliveira et al. 2019) and J-PLUS (Cenarro et al. 2018). Other surveys focused on Galactic and stellar science also have the necessity of classifying objects to obtain pure stellar samples, such as Pan-STARSS (Chambers et al. 2016) and Gaia survey (Gaia Collaboration 2016).

This task demands a particular approach since some of the aforementioned surveys have relatively large number of photometric bands and consequently it becomes a high-dimensional problem. Several classification algorithms have included photometric colours (e.g., Pollo et al. 2010; Kovacs & Szapudi 2016) and/or morphological parameters, such as extension and concentration index calculated, for instance, by **SEXTRACTOR** (Bertin & Arnouts 1996). Other works implemented a more complex approach on astronomical images, such as moment indices and granulometry (Candéas et al. 1997; Moore et al. 2006). As demonstrated in Pimblet et al. (2001), among several parameters, both the Full Width at Half Maximum (FWHM) and **SEXTRACTOR**'s stellarity parameter, provide a reliable morphological proxy to separate stars and galaxies.

Recently, several regressions and classification problems in Astronomy have started to be approached using an assortment of Machine Learning (hereafter ML) algorithms. They represent one of the main branches of this new generation of tools. They are able to identify complex nonlinear behavior in the multi-dimensional feature space, providing accurate solutions for several questions in Astronomy. Photometric redshifts (Cavuoti et al. 2014; Sadeh, Abdalla & Lahav 2016; Gomes et al. 2017; Bilicki et al. 2017) and galaxy morphological classification (Schutter&Shamir 2015; Barchi et al. 2017; Hocking et al. 2017; Domínguez Sánchez et al. 2018) are some examples which use ML. Particularly, the star/galaxy classification has been approached with several ML techniques, such as Support Vector Machines (SVMs) (Solarz et al. 2012; Fadely et al. 2012), Decision Trees and Random Forest (hereafter RF) (Breiman 2001; Odewahn et

al. 2004; Ball et al. 2006; Vasconcellos et al. 2011), Artificial Neural Networks (ANNs) (Qin et al. 2003; Bora et al. 2009; Kim & Brunner 2016). In particular, the **SEXTRACTOR** software is based on ANNs and widely used in astronomical images to classify stars and galaxies. Moreover, there are other techniques that tackle the star/galaxy separation in the literature, focused on SED-fitting (Wolf et al. 2004; Robin et al. 2007; Preethi et al. 2014), Bayesian statistics (Henrion et al. 2011; Molino et al. 2014; Lopez-SanJuan et al. 2018) and Principal Component Analysis (PCA) (Cabanac et al. 2002; Soumagnac et al. 2015). All these techniques have their strength and limitation, depending on the problem approached. Recently, Machado et al. (2016) evaluated a set of ML algorithms for the star/galaxy classification problem. The authors demonstrated that ANNs and RF performed better when compared to other methods, such as k-Nearest Neighbour (Bathia & Vandana 2010) and Naive Bayes (Jiang et al. 2007). In particular, the RF algorithm has some features which are suitable for the star/galaxy classification problem, i.e., the overfitting problem can be reduced and errors and probabilities are reliably calculated by averaging over a large enough number of trees (Robnik-Sikonja 2004; Boinee et al. 2005).

Here we present a star/galaxy separation technique based on the RF algorithm and its application to the S-PLUS data. This paper is organized as follows. In Section 2, we briefly introduce the S-PLUS survey, for which the work presented in this paper is meant to be applied to, given its filter system and photometric-depth. In Section 3, we present the RF algorithm which has been used to classify objects using the multi-band photometry and morphology as input features. Section 4 shows the performance (completeness, purity and misclassification) of the RF algorithm as a function of the apparent r-band magnitude and broad band colours. Section 5 presents some applications of the developed star/galaxy separation algorithm: a compiled point-source extragalactic catalogue. Then, in Section 6, our conclusions and discussions on the ML approach and results are presented.

The S-PLUS photometry presented here are in AB system. We have adopted the following cosmological parameters: $H_0 = 70 \text{ kms}^{-1} \text{ Mpc}^{-1}$, $\Omega_M = 0.3$, $\Omega_\Lambda = 0.7$ and $\Omega_K = 0.0$.

2 DATABASE

2.1 The S-PLUS survey

The Southern Photometric Local Universe Survey ¹ (S-PLUS; Mendes de Oliveira et al. 2019) is an ongoing photometric survey focused on Galactic science cases and will observe 9,000 sq. deg. of the Southern Hemisphere. The survey employs a dedicated 0.8m fully robotic telescope (T80-South) at Cerro Tololo, Chile. S-PLUS uses a 5 broad- and 7 narrow bands filter system in the optical, strategically designed to cover some stellar and galactic spectral features in the local Universe, such as metal-dependent features (e.g. Ca H+K and G band) and emission lines (e.g. H α and

¹ <http://www.splus.iag.usp.br>

[O II] $\lambda 3727$). Table 1 indicates their central wavelengths and widths.

The S-PLUS Data Release 1 (S-PLUS/DR1)² has observed the SDSS Stripe 82 (S82) region which covers the region at the Celestial Equator between $-1.25^\circ < \delta < +1.25^\circ$ and $-60^\circ < \alpha < +60^\circ$ (Jiang et al. 2014). The S-PLUS/DR1 data is composed by 170 fields, each one covering 1.96 sq. deg., and more than 2 million of objects up to $r=21$ mag.

In order to characterize the apparent morphology of objects, we used the following morphological parameters: the ellipticity defined as b/a (being a and b are the semi-major and semi-minor axes, respectively), a concentration proxy $C = r_{AUTO} - r_{PETRO}$, being the r magnitude using the AUTO (from SExtractor) and Petrosian (Petrosian 1976) formalism, and the full width at half maximum divided by the mean PSF (Point Spread Function) of the field. Our representative PSF definition consists of FWHM 5-th percentile value of objects in the magnitude range $14 < r < 17$, taking the bright magnitude range dominated by stars and relatively small FWHM in the field. All these parameters have been calculated from the detection images (see Sampedro et al in prep.). Since the FWHM is an observation-dependent parameter and so it is expected to vary from one field to another, so we decide to normalize this quantity by the PSF of the point-like source in the field. This approach allows us to define a more stable estimate of the FWHM of sources through the entire survey. In this way, point-like sources present values close to unity while extended sources have larger values.

Our initial magnitude-limited sample was extracted from the S-PLUS database between $14 < r < 21$ and matched with the SDSS Stripe 82 database, resulting in $\sim 924k$ objects in common for both catalogues. This photometric limit is defined to guarantee the balance between the photometric quality and depth in all bands. For our sample characterization, we selected all 12 S-PLUS bands (AUTO magnitudes) and the morphological parameters (FWHM/PSF, b/a and concentration) as input features for the ML algorithm. All objects in our initial sample have the SDSS/DR13 star/galaxy classification (Albaret et al. 2017). Furthermore, the SDSS Stripe 82 observations are deeper than S-PLUS data (SDSS data is complete down to $r=24.6$), so we have decided to rely on the SDSS star/galaxy classification as true for objects in this region and used its classification to train our algorithm. Thus, our goal in this work is to validate our classification by reproducing the SDSS classification from Stripe 82 for the S-PLUS survey and apply it on other S-PLUS fields in the future.

2.2 Training and Test samples

As a rule of thumb, supervised ML Algorithms are evaluated using an independent but representative sample compared to the training sample, called the test sample. The initial sample has been randomly split into training and test samples comprised of 724k and 200k objects respectively, to evaluate/validate the algorithm performance. Figure 1 shows the apparent magnitude (r band) distribution of initial sample (upper panel). It shows the dominance of stars/galaxies at

Table 1. Central wavelengths and widths of the S-PLUS filter system. For further details, we refer the reader to Mendes de Oliveira et al. (2019)

Filter Name	λ_{eff} [Å]	$\Delta\lambda$ [Å]	Spectral feature
uJAVA	3574	330	Javalambre u
F0378	3771	151	[O II]
F0395	3941	103	Ca H+K
F0410	4094	201	H δ
F0430	4292	200	G-band
gSDSS	4756	1536	SDSS-like g
F0515	5133	207	Mgb Triplet
rSDSS	6260	1462	SDSS-like r
F0660	6614	147	H α
iSDSS	7692	1504	SDSS-like i
F0861	8611	408	Ca Triplet
zSDSS	8783	1072	SDSS-like z

the bright/faint edge of our sample. The lower panel shows the fraction of objects as a function of missing bands, being 59% of the objects have all S-PLUS magnitudes measured, 20% of objects present one missing band and 21% have more than one missing band. We also characterize the distributions of stars and galaxies in the colour-colour space of the initial sample together. Figure 2 shows the *loci* of stars and galaxies in the colour-colour space using broad bands, adopting $(g-r)$ and $(r-i)$. Stars and galaxies present distinct distributions, however, there is an overlapping *locus*. This region may decrease our classification performance since there are objects from both classes occupying the same *locus*. On the other hand, it is important to mention that it shows simplified 2-dimensional distributions of stars and galaxies in colour-colour space. The RF analysis works in a higher-dimensional space, including more features than only two photometric colours.

3 METHODOLOGY

In this section, we describe the RF algorithm and how it is employed to classify objects as stars and galaxies based on S-PLUS magnitudes and morphological features.

3.1 Random Forest Algorithm

A diversity of topics can be investigated in Astronomy using ML such as galaxy morphology in seeing-limited images (Huertas-Company et al. 2009), classification of stars, galaxies and active nuclei (Zhang & Zhao 2005) and photometric redshift estimates (Wadadekar 2005). Particularly, the RF is frequently used in the astronomical context, dealing with high-dimensional data to classify or make regressions (e.g. Gao et al. 2009; O’Keefe et al. 2009; Vasconcellos et al. 2011; Machado et al. 2016; Baron & Poznanski 2017). The RF package from the library `scikit-learn`³ in Python (Pedregosa et al. 2011) was chosen for this work.

² <https://datalab.noao.edu/splus/index.php>

³ <http://scikit-learn.org/>

Here we briefly describe the RF algorithm, in particular, how the trees are built and trained (for more details, see Breiman 2001; Raileanu & Stoffel 2004). In the training procedure, the RF algorithm uses the training sample \mathcal{X} with M objects to create a number of trees (n_{tree}) bootstrapped subsamples \mathcal{S} with the same size as the initial sample \mathcal{X} . Due to the replacement (bootstrapped samples), objects can be duplicated in several subsamples. This procedure is known as *bagging*. Each tree can use at most a number of features (M_F), previously defined, randomly chosen for each tree to build themselves. This random subspace method guarantees that the classification of the algorithm is uniformly distributed over all trees and the entire forest works as a reliable classifier, instead of taking the classification from just one tree. Each bootstrapped subsample \mathcal{S}_i is used to build and train its respective i -th tree, passing through the tree as it grows.

During the tree growth, at the j -th tree node, the Gini impurity is used to measure the goodness of the classification. It is defined as,

$$\mathcal{G}_j = 1 - \sum_{k=1}^K p_k^2, \quad (1)$$

where K is the total number of classes and p_k represents the probability of observing the k -th class which is estimated as the fraction of objects of that class at the node. After the split at the j -th node (considering a certain feature and threshold value), those elements go down to one of the two child nodes, called left (l) and right (r) nodes, building up their child population N_l and N_r , respectively. The Gini impurity is then calculated at the child nodes assuming Eq. 1 for their respective object sets, i.e., \mathcal{G}_l and \mathcal{G}_r . The Information Gain (\mathcal{IG}) is then obtained after the node split by the difference between impurities at the parent and child nodes, weighted by their respective number of objects, i.e.,

$$\mathcal{IG}_j = \mathcal{G}_j - f_l \mathcal{G}_l - f_r \mathcal{G}_r \quad (2)$$

where f_l and f_r represent the fractions of objects at the child node related to the parent node. Note that if the child nodes are pure, i.e., if there is only one class at each child nodes, the child Gini impurity values are zero and $\mathcal{IG}_j = 0$ and it is not necessary to create new child nodes at that branch. These steps are taken to select the set of feature and threshold values that maximize \mathcal{IG} and provides the best and most efficient combination of feature and threshold value for the split at the node. This procedure is repeated for child nodes which are not pure and new child node are created, making the tree grows as the purity increases.

The tree growth happens until all leaves of the tree are pure or the minimum number of objects is reached, which in our case corresponds to two elements. Once all trees are built and trained using their respective subsamples \mathcal{S}_i , the RF is able to classify objects which are out of the training sample. Each tree outputs a classification label \mathcal{Y}_i for a certain object and the final class is denoted by the majority of the votes from all trees. In addition, the class probabilities are defined as the fraction of votes for each class.

The RF algorithm has a few free parameters to be defined for the training process and classification. The parameter n_{tree} has the major role in the RF multi-dimensional classification. The performance of the algorithm was conservatively evaluated as function of the n_{tree} and it has been

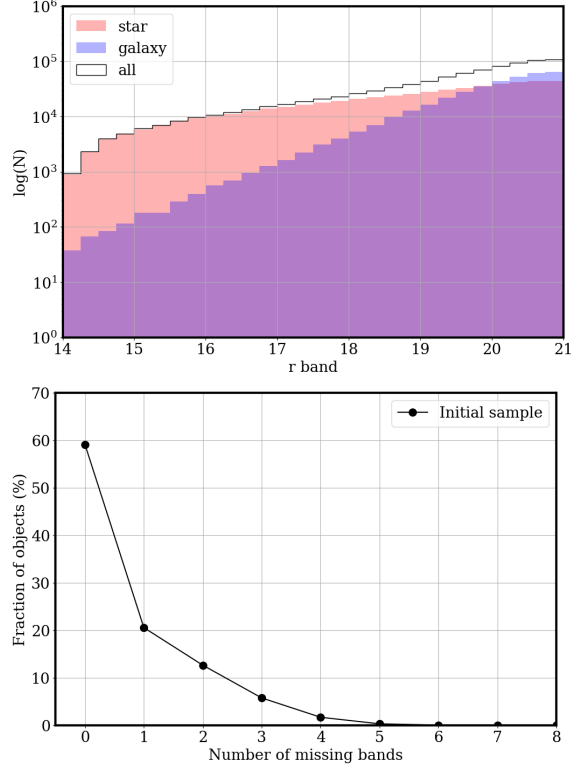


Figure 1. Content and photometric coverage of the initial sample. Upper panel: the r band distributions of objects classified as stars and galaxies according to the SDSS of the initial sample. Lower panel: the fraction of objects as a function of the number of missing bands. Both panels characterize our initial sample which was subsequently randomly split into training and test samples.

noticed that for $n_{\text{tree}} > 100$, our results are statistically stable, i.e., presenting similar performances. Thus, we adopt the n_{tree} of 300 ($n_{\text{tree}} = 300$). Other parametrizations were defined, for instance, the number of features used by each tree is defined by $\sqrt{N_F}$ as well as the metric for the node split is the Gini impurity (`criterion='gini'`) (Breiman 2001, for more details). All other scikit-learn parameters for the RF Classifier are set as default.

The RF as well as other ML algorithms are quite sensitive to incomplete datasets. This issue, known as the missing feature problem, has to be addressed in S-PLUS since sometimes sources are not detected in all bands simultaneously (see Section 2) and therefore, there is not available/missing information. Thus, several approaches have been proposed to circumvent the missing data problem adopting, for instance, simple median values or imputation-procedures (Schafer&Graham 2004; Rieger et al. 2010).

In this work, we have decided to be more conservative and train the RF algorithm for all combinations of missing features. In this way, our algorithm allows us to extract all information available for each object, independently of interpolations or assumptions which may not be correct. Initially, we consider the broad bands g , r , i and z bands as mandatory for the classification and all the others (uJAVA and narrow bands) may be missed. From 1 to 8 missing bands, the number of missing bands combinations are 255. Then 255 subsamples from the initial training sample were ex-

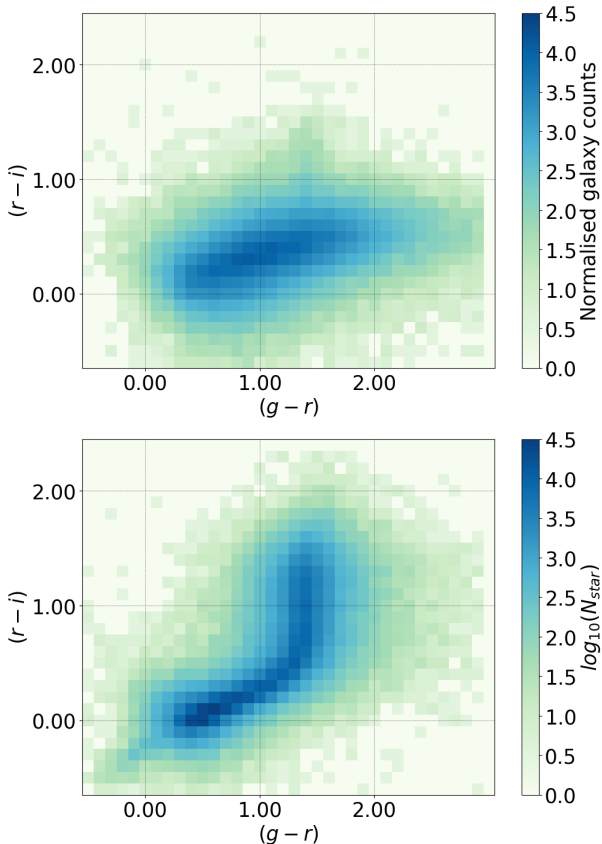


Figure 2. The *loci* of galaxies (upper panel) and stars (lower panel) in the colour-colour space $(g-r)$ versus $(r-i)$ of our initial sample. The classification shown here was extracted from the SDSS database.

tracted to train 255 RFs which represent all missing bands combinations. It is important to mention that the missing bands problem depends mainly on the apparent magnitude, i.e., fainter objects systematically present higher number of missing bands. Moreover, narrow bands are more affected at the faint edge of the sample due to their lower photometric signal-to-noise when compared to the broad ones. Subsamples used to train cases of missed narrow bands are consequently shallower than the initial training sample. These 255 subsamples cover distinct regions in the magnitude/colour space and their contents span between 214k and the initial 362k, according to their number of missing bands. The training subsamples are systematically larger as the number of mandatory bands decreases. All objects in our training sample present mandatory measured *griz* magnitudes. The training sample for this case is represented by the full case (362k). We trained RFs considering all 255 subsamples. The influence of the morphological parameters was evaluated by training RFs including (or not) those parameters. Therefore, we ended up with a total of 510 (255 missing bands combinations \times 2 configurations, with or without morphology features) trained RFs for all cases of missing bands and morphology parameters inclusion.

4 RESULTS

4.1 Completeness, Purity and Misclassification

After the training process, the performance of the trained RFs was evaluated using the test sample. We then define completeness as the fraction of correctly classified stars and purity is the ratio between the correctly classified stars and the total number of stars. Misclassification is the fraction of uncorrectly classified objects. Similarly, these parameters can also be implemented for galaxies. Since the initial training and test samples were randomly extracted from the S-PLUS database, it is expected that they occupy the same *locus* in the colour-colour space and suffer from the missing bands problem similarly.

Figure 3 shows the RF performance for the test sample, indicating the completeness, purity and misclassification of stars and galaxies as a function of the apparent *r*-band magnitude. Since S-PLUS/DR1 dataset up to now consists of a relatively small area in the sky, the number of bright galaxies is not enough to properly train the RF algorithm at that magnitude range. We decided to select solely those detections with a magnitude $r > 18$ (see also Figure 1), leaving the classification of very bright galaxy for future datasets.

When morphology is included in the features set (left panels in figure 3), the completeness and purity reach 85% or more for both classes down to $r=21$. The star completeness and purity systematically decline as they go to fainter magnitudes, as expected. However, the galaxy completeness and purity presented a roughly constant or at most slightly decreasing behaviour for fainter magnitudes. In average, the misclassification values for stars and galaxies are below 10% for the majority of the magnitude range. On the other hand, the RF performance for features set composed only by S-PLUS magnitudes (right panels in Figure 3) is systematically worse when compared to the morphology inclusion case. The star and galaxy completeness decreases down to 67% and 89% at the faint end, respectively. The misclassification presents values of 4% for stars and 11% for galaxies at $r=18$ and reaches values of 20% at $r=21$ for both classes when the morphology is not included.

The improved performance due to the inclusion of morphological parameters can be explained by the fact that galaxies frequently present FWHM/PSF values larger than unity while stars are point-like sources (FWHM/PSF \sim 1), which represents a good discriminant to separate these two classes. Particularly, in the faint end of the sample, the morphological parameters are crucial to separate galaxies and stars. Moreover, the SED characterization becomes less informative as it goes to fainter magnitudes due to the photometric noise and the systematically increasing number of missing bands. The RF algorithm employs the morphology of objects to improve the classification particularly for fainter objects. For the worst case scenario, having only the broad bands *g*, *r*, *i* and *z*, the accuracy is 94.8% and 82.5% when morphology is and not included, respectively.

4.2 Importance of Features

The RF algorithm also allows to estimate the importance of features, i.e., how discriminant or decisive a certain feature is on the RF classification. To evaluate the relevance

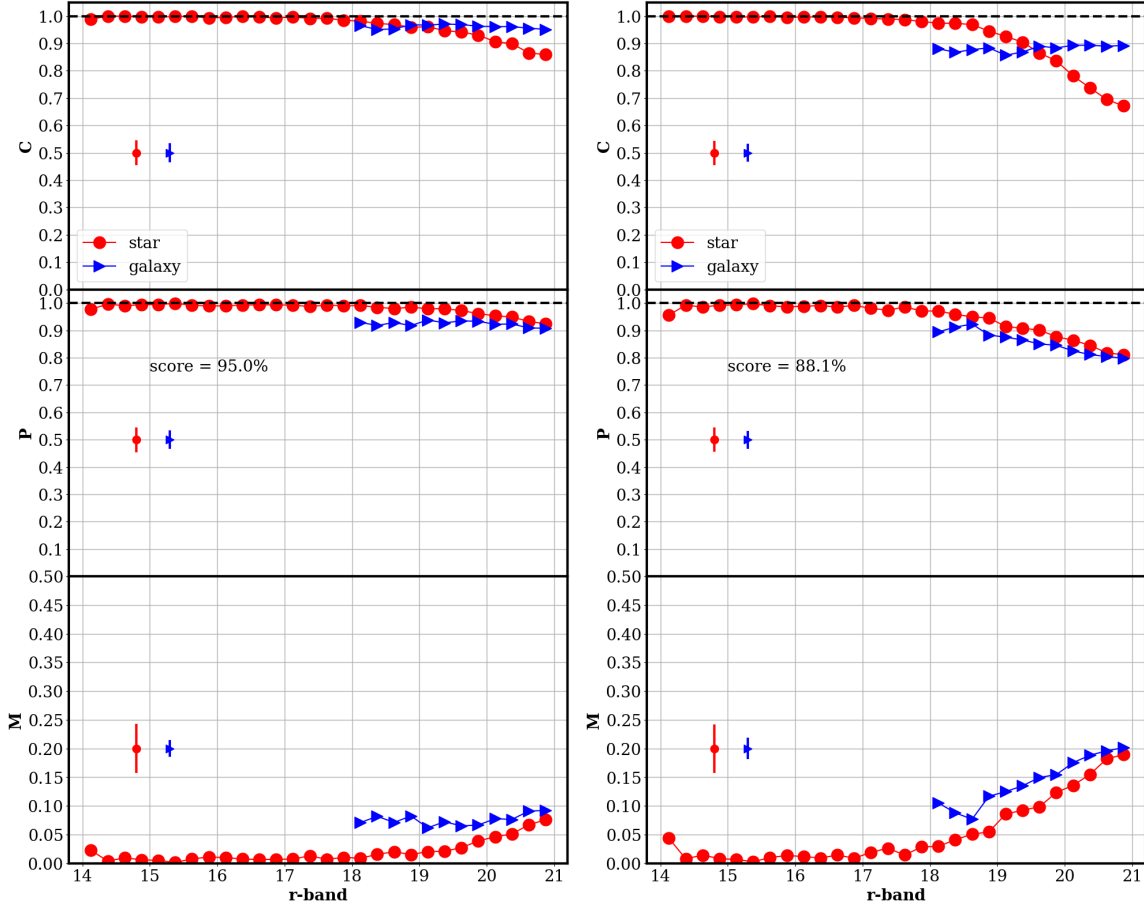


Figure 3. The Completeness (upper panels), Purity (middle panels) and Misclassification (lower panels) as function of r-band for stars (circles) and galaxies (triangles) from the test sample (see text). The left and right figures represent the cases in which morphology is or is not included, respectively. The typical error bars are shown at the left of each panel.

of each parameter, we define here the mean decrease accuracy. It is represented by the relative decrease in the initial accuracy ($acc_{initial}$) when all trends related to a certain feature vanish. The feature trends are erased by shuffling the values related to the feature in the test sample. All objects are then re-classified after the feature shuffle and a new accuracy of performance is calculated ($acc_{shuffled}$). Since there is no correlation with other features, the new accuracy is consequently lower. The importance of the feature is then represented by the relative decrease in accuracy, i.e.,

$$I = (acc_{initial} - acc_{shuffled}) / acc_{initial}. \quad (3)$$

Positive values of I indicate that the feature has some importance for the classification. Null values indicate that the feature has no contribution in the algorithm classification. Note that the sum of all importance values (I) is not necessarily equal to unity. We have evaluated the importance of features for three different classification cases: i) only mandatory bands ($griz$), ii) 12 S-PLUS bands and iii) 12 S-PLUS bands plus including morphological parameters.

Figure 4 shows the relative importance of features for the cases, i), ii) and iii). Regarding case i), we can notice the importance above 20% for all bands. The z band presented a slightly higher importance compared to the others. In case ii), we still notice the importance of mandatory bands in the

classification. The $F0410$ and $F0430$ bands are strategically located at the redder region of the spectral feature D_n4000 at the rest-frame. Since the SED of stars are namely at the rest-frame and galaxies are always redshifted, these bands are important tracers of D_n4000 of stars while most galaxies do not have their D_n4000 detected in those bands due to their redshifts. As a consequence, its importance is slightly higher when compared to the other narrow bands. Case iii) shows the inclusion of morphological parameters in the classification. Our result shows that the FWHM/PSF presents by far the largest importance, being more than 30%. It indicates the relevance of the morphology, particularly how extended objects appear to be classified as stars and galaxies. Besides this result, we can still see minor order importance for z and g . Previous works in the literature already pointed out to the importance of FWHM in classifying objects into stars and galaxies (e.g., Lopez-SanJuan et al. 2018).

4.3 The RF performance in colour-colour space

The performance of the RF algorithm in the colour-colour space was also evaluated in this work, presenting regions with higher or lower performance as function of two broad band colours. Mandatory bands are chosen here because are not significantly biased due to the photometric depth. Figure

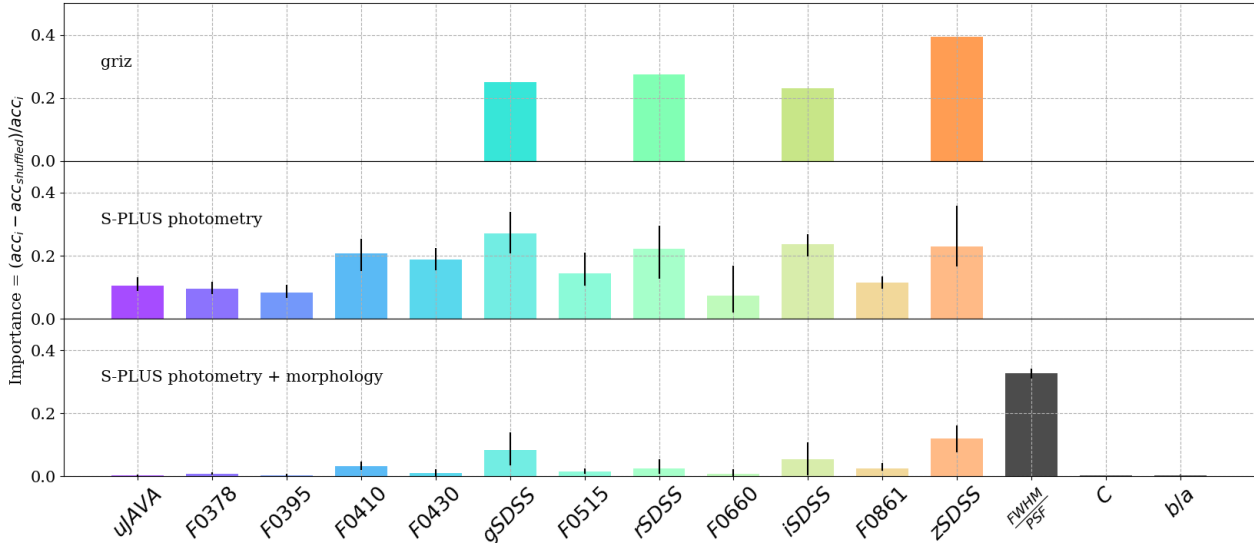


Figure 4. The importance of features is calculated using Eq. 3 for three set of features: only SDSS photometry (upper panel), S-PLUS photometry (middle panel) and S-PLUS photometry + morphology parameters (lower panel). The vertical black lines on the top of each bar represent 5% and 95% percentiles over all combinations of missing bands that include the feature.

5 shows the colour-colour space: $(g-r)$ versus $(r-i)$ containing galaxies and stars samples. The fraction of galaxies (upper panels), stars (lower panels) and their misclassification by using (or not) the morphology parameters are indicated by the colour maps. First, one can notice that stars and galaxies overlap in the colour-colour space. However, they prevail in distinct regions in such diagram (left panels). By comparing the fraction of galaxies or stars with their misclassification map in the colour-colour space, we notice a correlation between low fraction of objects and high misclassification. In regions which present galaxy fractions of 20% or lower, the misclassification of galaxies is higher than other regions. This correlation can be explained the low statistical significance of number of galaxies. In other words, when there is a large number of stars and low number of galaxies in a specific region in the diagram, the misclassification of galaxies at that region is more noisy due to the low number of objects of that class. The misclassification at those regions are shown in Figure 5, including only S-PLUS photometry (middle panels). Including morphological information in the RF algorithm, particularly the parameter FWHM/PSF, the misclassification decreases as a whole. In particular, regions with relatively high misclassification values due to the low number of objects of a certain class have their performance (lower misclassification) improved when the morphology is included (right panels).

Notably, galaxies with $(r-i) \sim 1$ and $(g-r) \sim 1.5$ do not present a significant improvement on classification with the morphology inclusion. At this region, one can notice that the number of galaxies is quite low when compared to the other ones, being probably the reason of no improvement.

4.4 What about QSOs?

Since QSOs are luminous, extragalactic and point-source objects, they are commonly classified as stars in most of star/galaxy classification algorithms. We evaluate our clas-

sification for these objects using a matched sample between the S-PLUS and the SDSS spectroscopic QSO confirmed objects, containing 8571 objects. Note that this spectroscopic sample is not complete due to the SDSS spectroscopic completeness when compared to S-PLUS photometric depth. However, this exercise is useful to show how our algorithm classifies QSOs.

The classification including morphology indicates that 18.9% of QSOs are classified as galaxies and 81.1% as stars. If we do not include morphological parameters, these numbers are 23.7% and 76.3%, respectively. The classification of QSOs as extragalactic objects is slightly better for the only photometry case but the majority of the QSOs are still classified as stars. It is important to mention that our classification reproduces the SDSS one. As the SDSS classifies most of QSOs as stars due to their point-source morphology, this caveat was expected. We present here a caveat of the algorithm on the QSO classification, reflecting a limitation of the training sample. On the other hand, it is not the scope of this work to classify QSOs. This problem will be tackled in other S-PLUS articles in the future (Nakazono et al., Queiroz et al., in preparation).

5 APPLICATIONS

5.1 The red galaxy sample contaminated by stars

Our results can also provide an estimate of the expected contamination rate in red galaxy samples by stars as a function of the redshift and colour. The assessment of stellar contamination is very important for cosmological studies such those on galaxy clustering. Such studies may employ contamination corrections on galaxy samples by specific types of object to remove systematic effects (e.g. Xavier et al. 2018; Peacock & Bilicki 2018). Moreover, the contamination estimate may help devise redshift and colour cuts that reduce the impact of such effects.

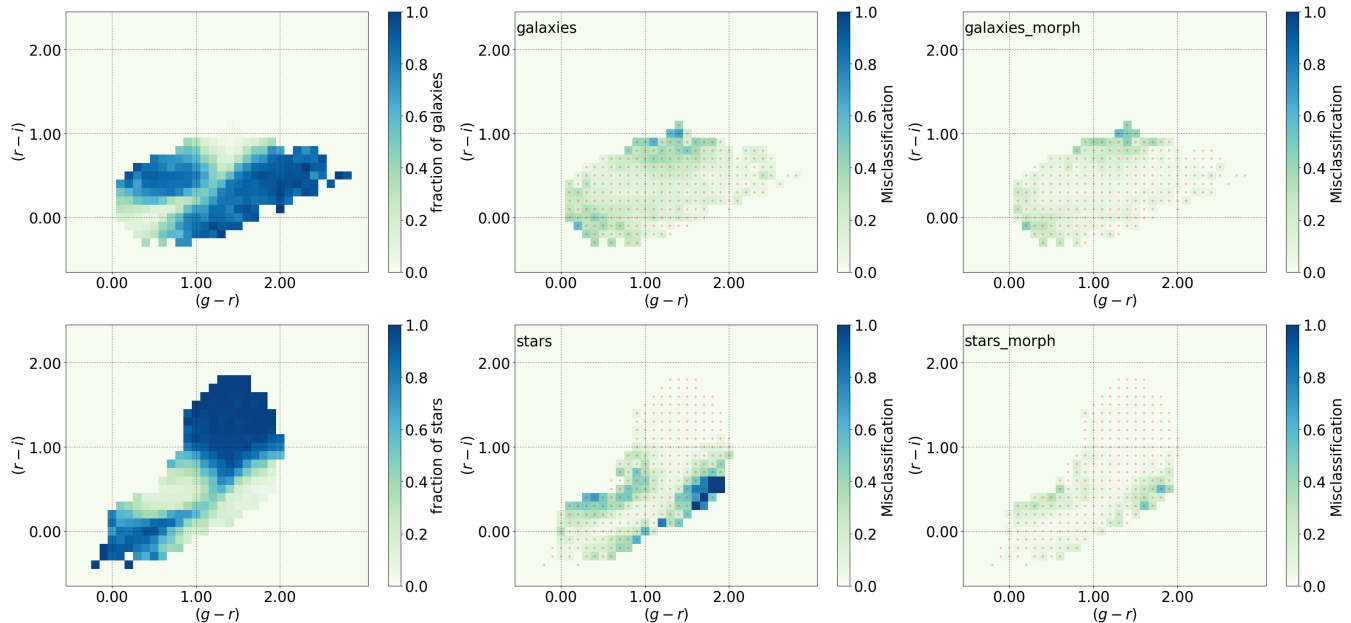


Figure 5. The colour-colour diagram ($g-r$) versus ($r-i$) for galaxies (upper panels) and stars (lower panels), showing the fraction of objects classified as galaxies and stars, misclassification using only S-PLUS photometry (middle) and the misclassification using S-PLUS photometry plus morphology (right). The misclassification was evaluated only for cells in the diagram which correspond to at least ten objects (red points in the middle and right panels).

We have estimated the stellar contamination fraction f_{star} in a galaxy sample using the following equation:

$$f_{\text{star}} = \frac{N_{\text{fake}}^g}{N_{\text{fake}}^g + N_{\text{real}}^g}, \quad (4)$$

where N_{fake}^g is the number of stars classified as galaxies and N_{real}^g is the number of correctly classified galaxies. Our estimate is presented as a function of colour in Figure 6 (upper panel). This estimate can serve as a guidance for the implementation of colour cuts aimed at improving the purity of a galaxy sample.

As an example, we have considered the case of luminous red galaxies (LRGs), which are frequently used in clustering analysis due to their high bias that eases the tracking of matter density contrasts. In order to simulate the expected colour evolution of an LRG in our colour-colour diagrams, we made use of the reddest galaxy template from the library of SED models of the Bayesian Photometric Redshift (BPZ2.0) code (Benítez 2000; Molino et al. 2017, 2018). We created a grid of SED models by redshifting the reddest galaxy template from $z = 0.00$ to $z = 0.45$ at steps of $dz = 0.01$. Then each SED model was convolved with our filter system in order to derive the expected model magnitudes in S-PLUS. This red galaxy track in the colour-colour diagram is presented in Figure 6, showing that this type of galaxy populates a region of low contamination rate.

Figure 6 (lower panel) shows the interpolated contamination rate for red galaxies as a function of redshift. We can see that our classification method reaches 5% contamination over the whole S-PLUS redshift range. As shown in Peacock & Bilicki (2018) and Xavier et al. (2018), such contamina-

tion level is low enough to allow the extraction of reliable cosmological parameters from the data.

5.2 The S-PLUS extragalactic point-source catalogue

The final product of this work is a star/galaxy classification for the S-PLUS catalog. As a subproduct, it provides a catalog of extragalactic point-source objects that are candidate to high- z galaxies, QSOs, compact HII galaxies and Ultra Compact Dwarf galaxies (UCDs). The classification only based on the S-PLUS photometry identifies objects classified as extragalactic ones, independently of the morphology (see Section 3.1).

Some constraints were imposed to select point-source and extragalactic objects:

- $14 < r < 21$
- $z_b > 0.002$
- $1.0 < \text{FWHM}/\text{PSF} < 1.5$
- $P_{\text{gal}} > 0.5$ (classified as galaxies)

where P_{gal} represents the probability of a certain object to be classified as a galaxy using the RF algorithm only based on 12 S-PLUS photometric bands. The photometric redshifts (z_b) were derived from Molino et al. (2019). Our initial catalogue contains roughly $\sim 18\text{k}$ objects. This extragalactic point-source catalogue will be explored in the future by the S-PLUS collaboration.

6 CONCLUSIONS

We present a star/galaxy classification for the S-PLUS project, based on the RF algorithm. This approach uses the

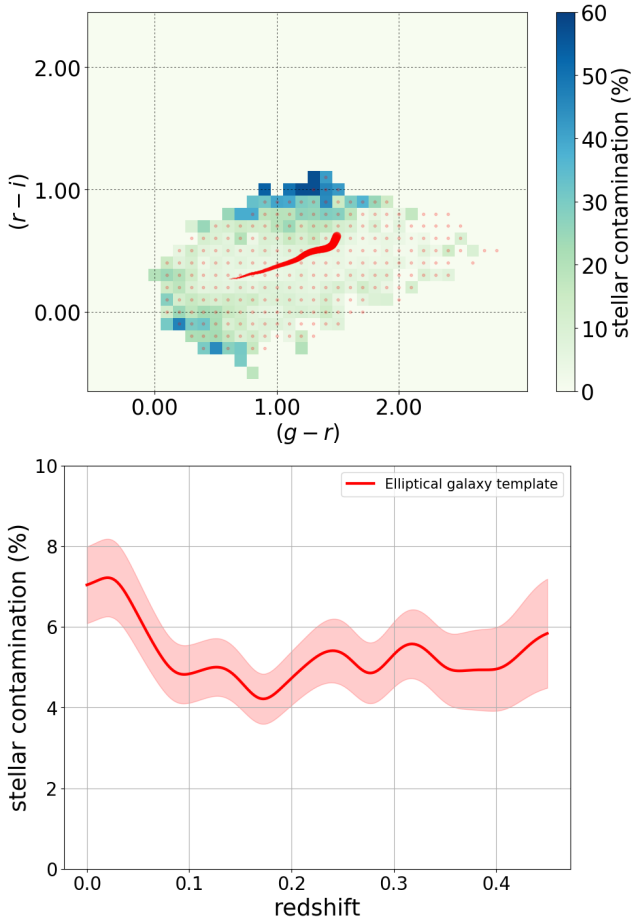


Figure 6. Upper panel: the stellar contamination in the colour-colour space $(g-r)$ versus $(r-i)$ associated to galaxies. It shows the redshift track of a red galaxy template convolved with the broad bands g , r and i up to redshift $z = 0.45$. Lower panel: the expected contamination by stars for a red galaxy sample as a function of the redshift. The shaded area represents 1σ uncertainties.

12 S-PLUS photometric bands as input for our classification. To evaluate the influence of the morphological information on the classification, we used two set of features. The first one consisting of only 12 all S-PLUS bands while the second one is represented by the 12 photometric bands and the morphological parameters, then we included and evaluated the impact of the following morphological parameters in the classification: full width at half maximum divided by the representative PSF of the field (FWHM/PSF), ellipticity (b/a) and concentration (C) at r band. The matched sample between the S-PLUS/S82 and SDSS/S82 was split into training and test samples, presenting 724k and 200k objects, respectively. To circumvent the missing bands issue in the S-PLUS, we trained several RFs for all combinations of missing bands. In total, 510 RFs were trained for all missing bands combinations and morphological information included or not. Our conclusions can be summarized as follows:

- Morphological information, in particular FWHM/PSF, is crucial for the star/galaxy classification. The performance of the algorithm with the inclusion of morphological information is considerably improved. The performance of the al-

gorithm is improved from an accuracy of 88.1% to 95.0% with the inclusion of the morphological information.

- The use of broad bands presented slightly larger importance when compared to the narrow ones due to their higher signal-to-noise, with one exception, the narrow band J0410 for the case when only 12 S-PLUS photometry is considered. This is one of the bands that traces the D_n4000 at the rest-frame, showing its importance to separate Galactic and extragalactic objects. Moreover, the FWHM/PSF presented the highest importance with more than 33% among all other features.

- We also presented the misclassification in the colour-colour diagram, showing the misclassification of stars and galaxies as function of two broad band colours, $(g-r)$ versus $(r-i)$. The classification improves due to the parameter FWHM/PSF, notably at the *locii* where the misclassification is relatively high. Regions where the classification is relatively uncertain when using only 12 S-PLUS bands had their misclassification decreased by including morphology information. One of the outputs is the stellar contamination (or misclassification) of a red galaxy sample as a function of redshift. This result can be useful for extragalactic studies.

The final product of this work is the classification of objects in the S-PLUS project as stars or galaxies. Also, we emphasize the importance of stellar contamination for extragalactic studies... etc.

- Another data product of this star/galaxy separation algorithm is the extragalactic point-source catalogue. The classification using only 12 S-PLUS bands and additional constraints on photo- z and FWHM/PSF values generates a sample with $\sim 18k$ objects, candidates for extragalactic point-source objects.

7 ACKNOWLEDGEMENTS

MVCD thanks the FAPESP scholarship process number 2014/18632-6 and 2016/05254-9. LS acknowledges the financial support of the FAPESP scholarship process number 2016/21664-2. We also thank the FAPESP thematic project number 2012/00800-4. FRH thanks FAPESP scholarship number 2018/21661-9. ACS acknowledges funding from the brazilian agencies *Conselho Nacional de Desenvolvimento Científico e Tecnológico* (CNPq) and the Rio Grande do Sul Research Foundation (FAPERGS) through grants CNPq-403580/2016-1, CNPq-310845/2015-7, PqG/FAPERGS-17/2551-0001. AAC acknowledges support from FAPERJ (grant E26/203.186/2016) and CNPq (grants 304971/2016-2 and 401669/2016-5). JLNC is grateful for financial support received from the GRANT PROGRAM FA9550-18-1-0018 of the Southern Office of Aerospace Research and development (SOARD), a branch of the Air Force Office of the Scientific Research International Office of the United States (AFOSR/IO).

This work has made use of the computing facilities of the Laboratory of Astrominformatics (IAG/USP, NAT/Unicisul), whose purchase was made possible by the Brazilian agency FAPESP (grant 2009/54006-4) and the INCT-A.

REFERENCES

- Abolfathi, B., Aguado, D. S., Aguilar, G., 2017, arXiv:1707.09322
- Dark Energy Survey Collaboration, 2017, Monthly Notices of the Royal Astronomical Society, 460, 1270
- Albaret, Franco D., Allende Prieto, Carlos, Almeida, Andres, Anders, Friedrich et al., 2017, ApJS, 233,25
- Ball, N. M., Brunner, R. J., Myers, A. D. et al., 2006, The Astrophysical Journal, 650, 497
- Barchi, P. H., da Costa, F. G., Sautter, R., 2017, arXiv:1705.06818
- Baron, D. and Poznanski, D., 2017, Monthly Notices of the Royal Astronomical Society, 465, 4530
- Bhatia, N. and Vandana, 2010, arXiv:1007.0085
- Benítez, N. 2000, ApJ, 536, 571
- Benitez, N., Dupke, R., Moles, M. et al., 2014, arXiv:1403.5237.
- Bertin, E. and Arnouts, S., 1996, A&AS, 117, 393
- Bilicki, M., Hoekstra, H., Amaro, V., 2017, arXiv:1709.04205
- Boinee, P., De Angelis, A., & Foresti, G. L., 2005, *International Journal of Computational Intelligence*, 2(3), 138-147.
- Bora, A., Gupta, R., Singh, H. P. et al., 2009, New Astronomy, 14, 649
- Breiman, L., 2001, "Machine Learning", 45, 5
- Gaia Collaboration, 2016, Astronomy & Astrophysics, 595, A2
- Candéas, A. J., Braga-Neto, U. M., Carvalho-Filho, E. C., 1997, J. Braz. Comp. Soc., vol.3, n.3
- Cabanac, R. A., de Lapparent, V. and Hickson, P., 2002, Astronomy & Astrophysics, 389, 1090
- Cavuoti, S., Brescia, M., Tortora, C., 2014, Monthly Notices of the Royal Astronomical Society, 452, 3100
- Cenarro, A. J., Moles, M., Cristóbal-Hornillos, D., 2018, arXiv:1804.02667
- Chambers, K. C., Magnier, E. A., Metcalfe, N. et al., 2016, arXiv:1612.05560
- Domínguez Sánchez, H., Huertas-Company, M., Bernardi, M. et al., 2018, Monthly Notices of the Royal Astronomical Society, 476, 3661
- Fadely, R., Hogg, D. W., Willman, B. et al., 2012, The Astrophysical Journal, 760, 15
- Faifer, F. R., Escudero, C. G., Scalia, M. C. et al., 2017, Astronomy & Astrophysics, 599, L8
- Gao, D., Zhang, Y.-X., Zhao, Y.-H., 2009, 9, 220
- Gomes, Z., Jarvis, M. J., Almosallam, I. A., et al., 2017, Monthly Notices of the Royal Astronomical Society, 475, 331
- Ivezic, Z., Tyson, J. A., Abel, B. et al., 2008, arXiv:0805.2366
- Henrion, M., Mortlock, D. J., Hand, D. J., 2011, Monthly Notices of the Royal Astronomical Society, 412, 2286
- Hilker, M., 2009, Reviews in Modern Astronomy, 21, 199
- Hocking, A., Geach, J. E., Sun, Y. et al., 2017, Monthly Notices of the Royal Astronomical Society, 473, 1108
- Huertas-Company, M., Tasca, L., Rouan, D. et al., 2009, Astronomy & Astrophysics, 497, 743
- Ilbert, O., Arnouts, S., McCracken, H. J., et al. 2006, A&A, 457, 841
- Ilbert, O., Capak, P., Salvato, M., et al. 2009, ApJ, 690, 1236
- Jiang, L., Wang, D., Cai, Z., et al., 2007, *Advanced Data Mining and Applications*, Springer, 2007, 134, 145
- Jiang, L., Fan, X., Bian, F. et al., 2014, ApJS, 213, 12
- Kim, E. J., Brunner, R. J., 2016, Monthly Notices of the Royal Astronomical Society, 464, 4463
- Kovács, A. and Szapudi, I., 2016, Monthly Notices of the Royal Astronomical Society, 448, 1305
- Little, R. J. A. and Rubin, D. B. *Statistical Analysis with Missing Data*, Wiley-Interscience, 2nd edition, ISBN 0471183865.
- López-Sanjuan, C., Vázquez Ramió, H., Varela, J., 2018, arXiv:1804.02673
- Machado E., Serqueira M., Ogasawara E., 2016, International Joint Conference on Neural Networks (IJCNN), 123, 1
- Mendes de Oliveira, C., Ribeiro, T., Schoenell, W., Kanaan, A., 2019, arXiv:1907.01567
- Mieske, S., Jordán, A., Côté, P. et al., 2006., The Astrophysical Journal, 653, 193
- Moles, M., Benítez, N., Aguerrí, J. A. L., 2008, AJ, 136, 1325
- Molino, A., Benítez, N., Moles, M., et al. 2014, MNRAS, 441, 2891
- Molino, A., Benítez, N., Ascaso, B., 2017, Monthly Notices of the Royal Astronomical Society, 470, 95
- Molino, A., Costa-Duarte, M. V., Mendes de Oliveira, C., 2018, arXiv:1804.03640
- Molino, A., Costa-Duarte, M. V., Sampedro, L. et al., 2019, arXiv:1907.06315
- Moore, J. A., Pimblett, K. A. and Drinkwater, M. J., 2006, Publications of the Astronomical Society of Australia, 23, 135
- Odehahn, S. C., de Carvalho, R. R., Gal, R. R. et al., 2004, AJ, 128, 3092
- O'Keefe, P. J., Gowanlock, M. G., McConnell, S. M., Patton, D., 2009, Astronomical Society of the Pacific Conference Series, 411, 318
- Peacock J. A., Bilicki, M., 2018, MNRAS, 481, 1133
- Pedregosa, F., Varoquaux, G., Gramfort, A. et al., Journal of Machine Learning Research, 12, 2825
- Petrosian V., 1976, ApJL, 209, L1
- Pimblett, K. A., Smail, I., Edge, A. C. et al., 2001, Monthly Notices of the Royal Astronomical Society, 327, 588
- Pollo, A., Rybka, P. and Takeuchi, T. T., 2010, Astronomy & Astrophysics, 514, A3
- Preethi, K., Gudennavar, S. B., Bubbly, S. G. et al., 2014, Monthly Notices of the Royal Astronomical Society, 437, 771
- Qin, D.-M., Guo, P., Hu, Z.-Y., 2003, Chinese Journal of Astronomy & Astrophysics, 3, 277
- Raileanu, L. E. and Stoffel, K., 2004, *Annals of Mathematics and Artificial Intelligence*, 41, 77
- Robertson, B. E., Ellis, R. S., Furlanetto, S. R., 2015, ApJL, 802, L19
- Robnik-Sikonja, M., 2004, *Lecture Notes in Computer Science*, 359, 370
- Refregier, A., Amara, A., Kitching, T. D. et al., 2010, arXiv:1001.0061
- Rieger, A., Hothorn, T., Strobl, C., 2010, *Random Forests with Missing Values in the Covariates*, Department of Statistics, University of Munich, Technical Reports, 79

- Robin, A. C., Rich, R. M., Aussel, H., 2007, ApJS, 172, 545
- Solarz, A., Pollo, A., Takeuchi, T. T., 2012, Astronomy & Astrophysics, 541, A50
- Sadeh, I., Abdalla, F. B. and Lahav, O., 2016, PASP, 128, 10
- Schafer, L. and Graham, J. W., 2004, *Missing data: our view of the state of the art.*, Psychol Methods, 147, 177
- Schutter, A., Shamir, L., 2015, 12, 60
- Soumagnac, M. T., Abdalla, F. B., Lahav, O., 2015, Monthly Notices of the Royal Astronomical Society, 450, 666
- Vasconcellos, E. C., de Carvalho, R. R., Gal et al., 2011, AJ, 141, 189
- Wadadekar, Y., 2005, PASP, 117, 79
- Wolf, C., Meisenheimer, K., Kleinheinrich, M. et al., 2003., Astronomy & Astrophysics, 421, 913
- York, D. G., Adelman, J., Anderson, Jr. et al., 2000, AJ, 120, 1579
- Zhang, H.-X., Peng, E. W., Cote, P. et al., 2015, VizieR Online Data Catalog, 180
- Xavier H. S., Costa-Duarte M. V., Balaguera-Antolínez A., Bilicki M., 2018, arXiv, arXiv:1812.08182
- Zhang, Y. and Zhao, Y., 2005, PASP, 115, 1006
- Zhang, Y. and Zhao, Y., 2014, ASPC, 485, 239